DAMAGE ASSESSMENT OF THIN WOVEN COMPOSITE SUBJECTED TO QUASI-STATIC TENSILE LOADING USING INFRARED THERMOGRAPHY

T. Lisle[1*], C. Bouvet[1], M. L. Pastor[1], P. Margueres[1], R. Prieto Corral[1]

[1]*Université de Toulouse ; INSA, UPS, Mines Albi, ISAE ; ICA (Institut Clément Ader) ; ISAE, 10, avenue Edouard Belin, 31055 Toulouse cedex 4, France.*
**teddy.lisle@isae.fr*

Keywords: woven composite, infrared thermography, heat source, energy release rate.

Abstract
In this study, an experimental approach for characterizing damage evolution on thin glass/epoxy woven composite using infrared thermography is presented. First, the damage scenario is investigated combining thermal field measurements and optical microscopic observations. Then, the surface temperature images are used to evaluate the dissipative heat source using the local heat diffusion equation, in the case of thin rectangular sample. Afterwards, a 2D spatial cartography of damage is obtained for different strain level, as well as an estimation of the energy release rate induced by transverse yarn microcracking. Finally the relevance of those experimental results is discussed by referring to the literature dealing with fracture toughness of woven composite.

1 Introduction

The application of woven fabric composites in engineering structures has been significantly increased due to attractive characteristics, such as excellent drapability over complex geometries, and their high damage tolerance. However, because of the complex inhomogeneous microstructure, the weave architecture, and disparate meso-consituent properties, the failure process of woven composite is complex and involves a multitude of fracture modes (matrix cracking, inter-yarn and intra-yarn cracking, inter-ply and intra-ply delamination). For the past decades, several authors have investigated the damage scenario of different woven composite laminates under quasi-static loading [1-3]. For woven carbon and glass fiber-reinforced composites, transverse matrix cracking is the first readily observable type of damage occurring during tensile loading.
Generally, damage in composite materials can be detected by non-destructive techniques (NDT) such as acoustic emission, radiography or ultrasonic C-scan technics, X-ray, vibration-based methods,... However for thin woven glass/epoxy composites those are mostly useless or too inaccurate to characterize damage such as intra-yarn matrix cracking. Thus NDT based on infrared thermography measurement can be used to characterize damage growth and heat dissipated energy, especially during fatigue testing [4,5]. Other authors used infrared thermography to investigate both damage location and dissipated thermal energy in metal materials, when the failure occurs [7].

In this paper, an experimental approach using digital infrared thermography to assess damage in thin woven glass epoxy composites is presented. This work is mostly based on the works of [7-10]. It particularly aims at studying the dissipative heat source distributions during traction testing. Thermal images are processed using the local heat diffusion equation to estimate the dissipative heat source distribution at all stages of damage. Afterwards, both damage evolution and dissipated energy induced by damage process are evaluated.
In a first part, after having presented the experimental arrangement, thermo-mechanical framework and infrared image processing used to estimate dissipative heat sources are briefly detailed. The second section deals with damage scenario characterization by comparing cumulated dissipative heat source distributions and optical micrographs. An estimation of the energy release rate induced by transverse yarn cracking is then presented. Finally results are discussed with regard to literature.

2 Experimental procedures

2.1 Material and manufacture

The material studied is a glass/epoxy (913-45%-7781) woven composite. The laminates are made of 8-harness satin balanced woven fabric prepegs plies with a fiber volume fraction of 50%. The yarn size is 0.5 mm width and 0.1 mm thickness. 8-harness satin weaves exhibit ply asymmetry with one side predominately warp and the other predominately weft (Figure 1. (a)). Mechanical properties of the laminate are summarized in Table 1. All samples are made of two prepregs plies with aligned warp direction. They are always manufactured with the warp woven face on the top of the thickness. The top face is so a warp side and the underside face a weft one. In this paper, an orthotropic laminate with the warp yarns of woven plies in the tensile direction will be noted as $[0°]_2$. As shown on the Figure 1 (c), the specimens were 30 mm wide and 0.33 mm thick with an approximate length of 150 mm between the tabs.

Young's modulus in wrap direction, $\mathbf{E_y}$ **(GPa)**	**21.5**
Young's modulus in weft direction, $\mathbf{E_x}$**(GPa)**	**20.5**
Shear modulus, $\mathbf{G_{xy}}$**(GPa)**	**3.5**
Poisson ratio, $\boldsymbol{\nu_{xy}}$	**0.15**
Thermal conductivity in wrap and weft direction, $\mathbf{k_{xx}}$, $\mathbf{k_{yy}}$ **(W.m^{-1}.K^{-1}) -** [11]	**0,55**
Specific heat, $\mathbf{C_p}$ **(J.kg^{-1}.K^{-1})** - [6]	**882**
Density, **ρ (kg.m^{-3})**	**1730**

Table 1. Mechanical and thermal properties of a glass/epoxy woven laminate.

2.2 Tests setup

The specimens were tensile loaded with the warp yarns of woven plies lined up with the tensile direction. Traction tests were performed on an electromechanical tension machine (INSTRON, capacity: 10kN) at room temperature, with a crosshead speed of 20 mm.min^{-1}. A multi-detector infrared camera (FLIR SC7000 MW) was used to monitor the thermal response of the sample surface during experiments. The infrared camera has a maximum resolution of N_x x N_y = 320 x 256 pixels and a thermal resolution of 0.025 K for relative temperature measurement. The spatial resolution (pixel size), determined by the focal distance, is set to 0.17 mm (maximum magnification of the lens) in order to have at least 3 pixels by yarn. Thermal images were recorded at a frequency of 50 Hz. In order to avoid thermal perturbations arising from external environment, the specimens were enclosed in a rectangular box made of expansive foam. This box was painted in black inside and covered with a black opaque fabric outside, (Figure 1 (b)).

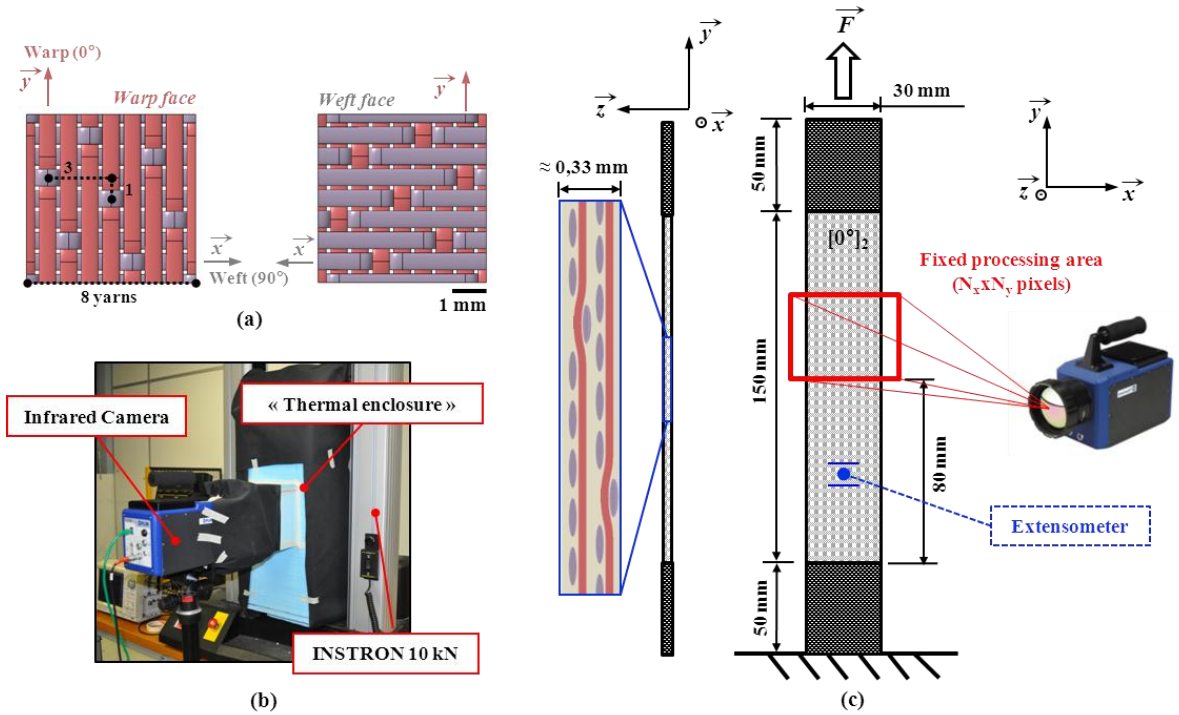

Figure 1. (a) Schematic representation of 8-harness satin glass/epoxy laminate. **(b)** Photography of the experimental setup. **(c)** Specimen geometry, position of the fixed processing area and position of the extensometer.

The face of sample monitored by infrared camera was covered with a thin layer of black paint to maximize the surface emissivity (>0.96). As previously mentioned, transverse yarns microfractures is the main observable damage in satin woven composite [1-3]. Hence, in this study, in order to accurately capture the temperature changes induced by transverse yarns microcracking, the sample face observed with the infrared camera was the weft face. To estimate the global strain, an extensometer was sticked on the sample warp face, (Figure 1 (c)).

2.3 Heat source evaluation by infrared thermography

Because of thermal transfer processes (internal conduction, convection with external environment, …), surface temperature measurement can be tricky to interpret. However, thermal fields measurements of the sample surface could be used to estimate the internal heat source distribution associated with a temperature distribution. The methodology used here is founded on the previous work of Chrysochoos et al. [7-9]. Using the framework of irreversible thermodynamics, the authors have presented a methodology to estimate internal heat source, starting from the heat diffusion equation. This technic, developed for isotropic thin sheet sample, has been used to study the dissipative phenomena during necking localization in steels [7,8] or in semi-crystalline polymers [9]. For such sample geometry, temperature and internal heat source are supposed to be homogeneously distributed through the thickness. More details about thermodynamics framework and mechanical assumptions of the methodology used in this study can be found in [7].

In what follows, specimens are considered as thin orthotropic sheets. Such an assumption involves that the coupling terms in the symmetric thermal conductivities matrix, k_{xy}, k_{xz} and k_{yz} are zero [16]. Thus, under the consideration of mechanical and thermodynamic quasi-static processes, the heat diffusion equation integrated through the thickness can be expressed as follow:

$$\rho C \frac{\partial \theta}{\partial t} - \left[k_{xx} \frac{\partial^2 \theta}{\partial x^2} + k_{yy} \frac{\partial^2 \theta}{\partial y^2} \right] + \frac{\theta}{\tau_{th}} = W_{hs} \quad (1)$$

Where ρ is the mass density and C is the specific heat. k_{xx} and k_{yy} are respectively the thermal conductivity in the weft and warp directions. τ_{th} represents a time constant characterizing the heat losses perpendicular to the sample surface (z direction). $\theta = T(x,y,t) - T_0(x,y)$ denotes the temperature variation averaged across the thickness between current and initial equilibrium states, while W_{hs} is the average volume heat source (in $W.m^{-3}$) crosswise the thickness. In this study thermo-mechanical coupling (principally thermoelastic coupling) were neglected. Such an assumption is reasonable considering quasi-static evolution and small temperature variation. Thereby, the volume heat source W_{hs} is directly equal to the intrinsic mechanical dissipation per unit volume [7-9].

Using thin sheet sample assumption, the average temperature *T(x,y,t)* can be estimated from surface temperature measurement. Thus, the volume heat source W_{hs} can be directly obtained from an estimation of the left-hand member of equation (1), for each fixed pixel position *(x,y)* at any time *t*. However, as differential operator estimations from noisy data are tricky, thermal images were filtered before the estimation of derivatives. In this work noisy thermal images were locally fitted by a parabolic surface function (2D second order polynomial), by using a linear least-square method. The size of approximation zone has to be large enough to filter the noise and small enough to detect small heterogeneous heat sources. Numerical tests were conducted to get a good compromise between these two criterions, as a reasonable calculation time. Finally, an approximation zone of 5x5 square pixels was chosen to filter thermal data.

3 Results and discussions

3.1 Damage behavior of 8-harness woven laminates - $[0°]_2$

As previously mentioned, observation of the tested laminates were performed using Scanning Electron Microscopy (SEM) after having cut and polished a selected piece of the tested sample, (Figure 2. (b)). Tensile tests were performed and stopped at different strain levels to perform optical micrographs. The stress-strain curves and corresponding optical micrographs are respectively shown on Figure 2. (a) and Figure 2. (c). Transverse fracture of the weft yarns was the first observed damage, as referred in the literature by several authors [1-3]. Initiation of the weft yarn fracture was considered by Osada et al. [1], to be caused by the bending deformation of the weft fiber bundle. Indeed, when the warp yarn is subjected to tensile deformation, bending deformation appears in the weft fiber bundle, which then leads to the transverse microfracture of the yarn.

Figure 2. (c) shows that microcracking of the weft yarns occurs around the well know “knee point”, and afterwards both the length and the number of microcracks in the yarn extend with increasing the strain. Moreover, as it is shown on the magnification of picture (C), microfractures extend in the weft direction at the fiber / matrix interface. Finally, the total failure of the specimen occurred when ultimate tensile strength of the warp fiber bundle is reached. Hence, as observed on the post-mortem micrographs D and D’, multiple fractures appear along all the fiber in the warp yarns (picture D’).
Furthermore, picture D shows that transverse microfractures extend toward the cross-over points of the woven plies. These observed fracture bifurcations can be linked to the fact that the cross-over points constitute ideal places for fiber yarn failure.

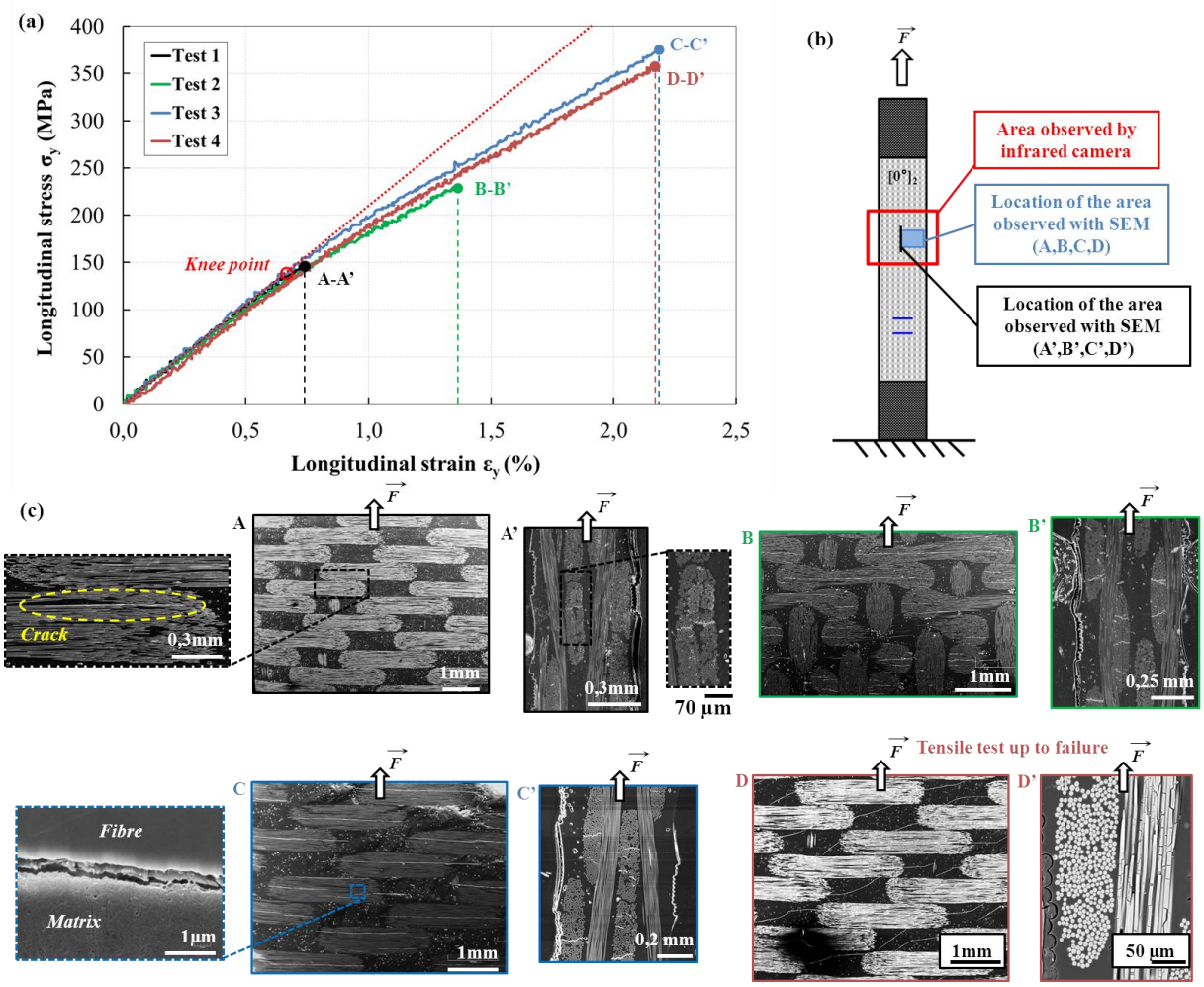

Figure 2. (a) Stress–strain curves of warp direction tensile tests, $[0°]_2$. **(b)** Location of the observed areas. All observations are realized on the weft face with SEM. **(c)** Optical micrographs at different strain states corresponding to points A-A', B-B', C-C' and D-D' on the stress-strain curves.

Figure 3. (b) shows the temperature variation fields of the whole zone observed at a strain level of 1.4%. Several thermal patterns are clearly identifiable. Magnification of one of these thermal signatures and the corresponding heat source fields evolutions are presented on Figure 3. (d)-(e). As it can be seen, during fracture yarn propagation, localised dissipative heat source expands sharply in the weft tow (during two images ≈ 0.04 s). Due to thermal diffusivity, temperature rising in the yarn arises one image (0,02s) after the heat source appearance. Furthermore, the dissipative heat source fields represented in Figure 3. (e) reveal the presence of diffuse damage propagation into the whole width of the weft yarn during crack growth.

Thereafter, a spatial cartography of whole transverse microfractures can be obtained at any level of strain by temporally cumulating heat sources detected on each image pixels. Figure 4 presents the total cumulative energy E_{tot} ($J.m^{-3}$) cartography for three different stages of damage. E_{tot} was calculated using the following equation:

$$E_{tot}(x,y) = \int_0^{t_{tot}} W_{hs}(x,y,t)\, dt \qquad (2)$$

Where t_{tot} represents total integration time.

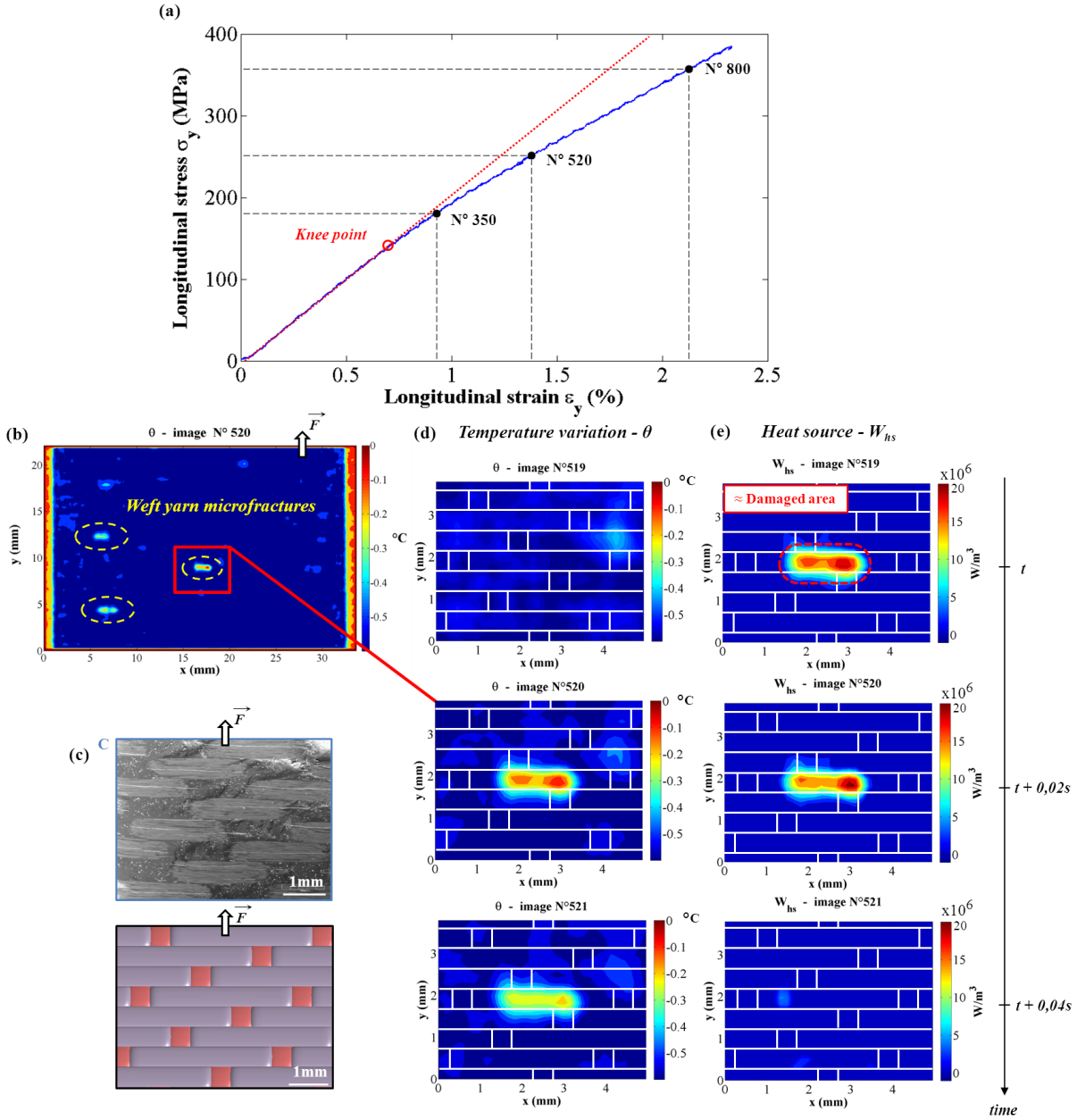

Figure 3. (a) Stress–strain curve indicating selected pictures. **(b)** Temperature variation fields of the whole observed zone. **(c)** Optical micrograph C and schematic representation of the weft face. **(d)** Temperature variation fields and **(e)** corresponding heat source fields with the weave pattern of the weft face layered.

According to optical micrographs previously presented and to the images N°350 and N°520 transverse yarn fractures appear gradually in several weft yarns starting from the knee point. Finally, image N°800 shows that close to the final failure, most of the weft yarns exhibit microfractures.

3.2 Energy release rate by weft yarn microcracking

Since the experimental heat sources can be directly linked to the dissipative mechanical power, an estimation of the energy release rate by transverse yarn microfracture G_{Ic} can be obtained from the following equation:

$$G_{IC} = \frac{1}{\beta S_f} \int_t \left(\int_V W_{hs}(x,y,t) dv \right) dt \quad (3)$$

Where, S_f is the fractured surface estimated by combining heat sources fields and optical micrographs. V represents the total damaged volume, which is equal to the damaged area represented on Figure 3. (e), multiplied by the thickness of the sample. β denotes the ratio of mechanical energy converted into heat. Assuming, in a first approximation, that all the mechanical energy is converted into heat, i.e. β=1, a lower bound of the critical energy release rate G_{Ic} is obtained: G_{Ic} = 0.40 kJ.m^{-2}, which is in the same range as these reported in table 2.

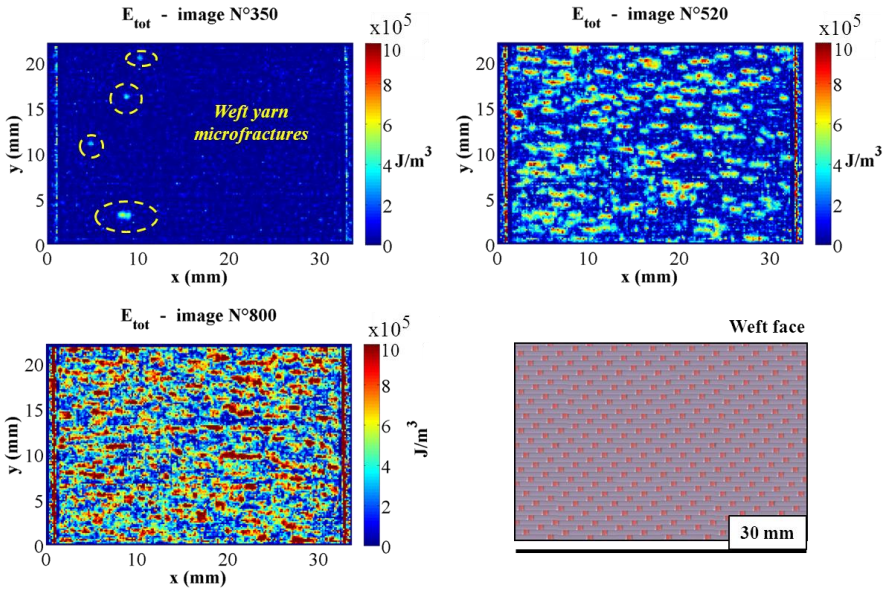

Figure 4. Total cumulated energy for selected pictures and schematic representation of the weft woven face.

However, due to disparate material properties and different local crack paths for each woven fabric, these results are difficult to compare. Furthermore, microfractures appear only in the weft yarn, which represents approximately the half of the ply thickness. Thus assuming homogeneous heat sources through the thickness of the sample may be unsuitable. Several studies are currently in progress to evaluate the relevance of the assumptions used and to identify a suitable value for β. Consequently, an estimation of the energy rates dissipated trough heat and through new surfaces creation should be obtained.

Weave structure	Material	G_{Ic} (kJ.m^{-2})	Reference
4 HS woven	Glass-fiber/epoxy (EE190ET442)	0.67-0.96	[12]
5 HS woven	Carbon-fiber/epoxy	0.43-0.87	[13]
8 HS woven	Glass-fiber/epoxy (LY1802/HY2954)	0.77-0.91	[14]
Unidirectional	Carbon-fiber/epoxy (T300/913)	0.21	[15]

Table 2. Mode I interlaminar fracture toughness of woven composites and mode I intralaminar fracture toughness of carbon/epoxy unidirectional laminated composites.

Conclusion

Damage scenario of $[0°]_2$ 8 harness satin woven laminate was investigated up to failure, combining optical micrographs and dissipative heat sources fields calculated from thermal images. Transverse weft yarn fracture was confirmed to be the main damage in harness satin woven composite, as referred in the literature. Afterwards, a methodology to estimate the

energy release rate by transverse microcracking has been proposed and shows high potential. However, energy dissipated through new surfaces creation in relation to the heat and total energy cannot be deduced from this experimental study so far. Thus, to figure out each energy ratio, an experimental study will be conducted on mode I translaminar fracture toughness of $[0°]_2$ woven composite laminates. Despite the relative relevance of the energy release rate estimated, infrared thermography seems to be a powerful technic to monitor damage in thin glass/epoxy woven laminate during loading.

References

[1] Osada T., Nakai A., Hamada H. Initial fracture behavior of satin woven fabric composites. *Composites Structures*, **61**, pp. 333-339 (2003).
[2] Daggumati S., De Baere I., Van Paepegem W., Degrieck J., Xu J., Lomov S.V., Verpoest I. Local damage in a 5-harness satin weave composite under static tension: Part I - Experimental analysis. *Composites Science and Technology,* **70**, pp. 1926-1933 (2010).
[3] Gao F., Boniface L., Ogina S.L., Smith P.A., Greaves R.P. Damage accumulation in woven-fabric CFRP laminates under tensile loading: Part 1. Observations of damage accumulation. *Composites Science and Technology,* **59**, pp. 123-136 (2012).
[4] Toubal L., Karama M., Lorrain B. Damage evolution and infrared thermography in woven composite laminates under fatigue loading. *International Journal of Fatigue*, **28**, pp.1867–1872 (2006).
[5] Naderi M., Kahirdeh A., Khonsari M.M. Dissipated thermal energy and damage evolution of Glass/Epoxy using infrared thermography and acoustic emission. *Composites: Part B*, **43**, pp. 1613-1620 (2012).
[6] Emery T.R., Dulieu-Barton J.M., Earl J.S., Cunningham P.R. A generalised approach to the calibration of orthotropic materials for thermoelastic stress analysis. *Composites Science and technology*, **68**, pp. 743-752 (2008).
[7] Chrysochoos A., Louche H. An infrared image processing to analyse the calorific effects accompanying strain localisation. *International Journal of Engineering Science*, **38**, pp. 1759-1788 (2000).
[8] Dumoulin S., Louche H., Hopperstad O.S., Børvik T.. Heat sources, energy storage and dissipation in high-strength steels: Experiments and modelling. *European Journal of Mechanics A/Solids*, **29**, pp. 461-474 (2010).
[9] Wattrisse B., Muracciole J.-M., Chrysochoos A. Thermomechanical effects accompanying the localized necking of semi-crystalline polymers. *International Journal of Thermal Sciences*, **41**, pp. 422-427 (2002).
[10] Oleg I. Benevolenski, József Karger-Kocsis, Tibor Czigány, Gábor Romhány. Mode I fracture resistance of glass fiber mat-reinforced polypropylene composites at various degree of consolidation. *Composites: Part A*, **34**, pp. 267-273 (2003).
[11] Bigaud D., Goyhénèche J.-M., Hamelin P. A Global-local non-linear modelling of effective thermal conductivity tensor of textile-reinforced composites. *Composites: Part A*, **32**, pp. 1443-1453 (2001).
[12] Pereira A.B., De Morais A.B., De Moura M.F.S.F., Magalhães A.G. Mode I interlaminar fracture of woven glass/epoxy multidirectional laminates. *Composites: Part A*, **36**, pp. 1119-1127 (2005)
[13] Gill A. F., Robinson P., Pinho S. Effect of variation in fibre volume fraction on modes I and II delamination behaviour of 5HS woven composites manufactured by RTM. *Composites Science and Technology*, **69**, pp. 2368-2375 (2009).
[14] Alif N., Carlsson L.A., Boogh L. The effect of weave pattern and crack propagation direction on mode I delamination resistance of woven glass and carbon composites. *Composites Part B*, **29B**, pp. 603–611 (1998).
[15] Pinho S.T., Robinson P., Iannucci L. Developing a four point bend specimen to measure the mode I intralaminar fracture toughness of unidirectional laminated composites. *Composites Science and Technology*, **69**, pp. 1303-1309 (2009).
[16] Daxu Zhang, Hayhurst D.R. Influence of applied in-plane strain on transverse thermal conductivity of 0°/90° and plain weave ceramic matrix composites. *International Journal of Solids and Structures*, **48**, pp. 828-842 (2011).